

Taylor & Francis
Taylor & Francis Group

Molecular Physics

An International Journal at the Interface Between Chemistry and Physics

ISSN: 0026-8976 (Print) 1362-3028 (Online) Journal homepage: www.tandfonline.com/journals/tmph20

Precision measurement of the ionisation energy of the $3d\sigma\ GK$ state of H_2

D. Sprecher, M. Beyer & F. Merkt

To cite this article: D. Sprecher, M. Beyer & F. Merkt (2013) Precision measurement of the ionisation energy of the $3d\sigma\ GK$ state of H_2 , Molecular Physics, 111:14-15, 2100-2107, DOI: 10.1080/00268976.2013.788743

To link to this article: https://doi.org/10.1080/00268976.2013.788743

Published online: 01 May 2013.

Submit your article to this journal

Article views: 346

View related articles

Full Terms & Conditions of access and use can be found at
https://www.tandfonline.com/action/journalInformation?journalCode=tmph20

Molecular Physics, 2013
Vol. 111, Nos. 14–15, 2100–2107, http://dx.doi.org/10.1080/00268976.2013.788743

Taylor & Francis
Taylor & Francis Group

INVITED ARTICLE

Precision measurement of the ionisation energy of the $3d\sigma\ GK$ state of H_2

D. Sprecher, M. Beyer and F. Merkt*

Laboratorium für Physikalische Chemie, ETH Zürich, Zurich, Switzerland

(*Received 10 January 2013; final version received 13 March 2013*)

The frequency of the transition between the $3d\sigma\ GK\ ^1\Sigma_g^+$ ($v = 1$, $N = 1$) state of H_2 and the $n = 56p$ ($N = 1$, $S = 0$) Rydberg state belonging to a series converging to the $X^+\ ^2\Sigma_g^+$ ($v^+ = 0$, $N^+ = 1$) ground state of ortho H_2^+ has been measured with an accuracy of 1.2 MHz using a narrow-band pulsed near-infrared (NIR) laser. Systematic errors originating from ac and dc Stark shifts, from pressure shifts and from the frequency shift and chirp accompanying the generation of the NIR laser pulses were quantified. By combining this frequency with the binding energy of the $56p$ ($N = 1$, $S = 0$) Rydberg state, the ionisation energy of the $GK\ ^1\Sigma_g^+$ ($v = 1$, $N = 1$) state of ortho H_2 was determined to be 379855188.3(12) MHz [12670.60522(4) cm^{-1}]. This new result represents the first step towards the determination of the ionisation and dissociation energies of molecular hydrogen at a $\nu/\Delta\nu$ level of accuracy beyond 10^{10}. Using the current value of the ionisation energy of ortho H_2 [124357.23797(36) cm^{-1}, from Liu *et al.* [J. Chem. Phys. **130**, 174306 (2009)] and the frequency interval between the $N = 1$ and $N = 0$ rotational levels of the $X(v = 0)$ ground state of H_2 [118.48684(10) cm^{-1}, from Jennings *et al.* [J. Mol. Spectrosc. **126**, 19 (1987)], the term value of the $GK\ ^1\Sigma_g^+$ ($v = 1$, $N = 1$) state was determined to be 111805.1196(4) cm^{-1}.

Keywords: molecular hydrogen; precision measurement; *GK* state; Rydberg states; ionisation energy; dissociation energy

1. Introduction

Precision measurements of energy intervals in atoms and molecules by high-resolution spectroscopy play an important role in the natural sciences: they help to study the fundamental laws and the fundamental symmetries in nature [1]. They provide rigorous tests of existing theories and, when necessary, they stimulate the development of new theories. For example, the discovery by high-resolution spectroscopy of a splitting between the $2s\ ^2S_{1/2}$ and $2p\ ^2P_{1/2}$ states of atomic hydrogen, by Lamb and Retherford [2], led to the development of modern quantum electrodynamics (QED) as an extension of Dirac's relativistic quantum theory. The measurement of a possible electric dipole moment of the electron by high-resolution spectroscopy of diatomic molecules such as YbF [3] and the study of space inversion symmetry by high-resolution spectroscopy of chiral molecules [4] represent two examples where the study of molecular systems may provide information relevant in the context of the standard model of particle physics and its extensions. The complete interpretation of the corresponding spectroscopic results will necessitate an accurate description of molecular structure, which include effects beyond the usual treatment of molecular structure based solely on electromagnetic interactions and the Born–Oppenheimer approximation.

Precision measurements of the ionisation and dissociation energies provide rigorous tests of *ab initio* calculations of molecular structure which include adiabatic and non-adiabatic corrections to the Born–Oppenheimer approximation and QED corrections. H_2 and its isotopomers, HD and D_2, are the simplest molecules displaying all features of a chemical bond, including electron correlation. Because molecular hydrogen has only two electrons, the Born–Oppenheimer electronic potential energy functions of the lowest electronic states, and the adiabatic and non-adiabatic corrections can be calculated with very high accuracy using well-established procedures [5–8], and QED corrections of progressively higher order in the fine-structure constant α can be evaluated in a perturbative treatment [5,8,9].

The current status of the comparison of experimental and theoretical values of the dissociation and ionisation energies of H_2, HD and D_2 is that they agree within the combined uncertainty of 30 MHz of the theoretical and experimental determinations (see Ref. [10], and references cited therein). To reach this agreement, the leading (one-loop) term of the α^4 QED correction term had to be evaluated for the first time in a molecular system with more than one electron [5,9]. Experimental results of a still higher precision are required to test future calculations of the full α^4 term and terms of higher order in α, and assess the convergence of the expansion in α.

Our approach to measure the dissociation energy D_0 of H_2 is to measure the ionisation energy E_I of H_2 and use a thermodynamical cycle to relate E_I and D_0 [10,11]. This

*Corresponding author. Email: merkt@phys.chem.ethz.ch

© 2013 Taylor & Francis

approach does not rely on the detection of the onset of dissociation or ionisation continua in the spectrum of molecular hydrogen, but on the measurement of the transition frequencies to *np* Rydberg states belonging to series converging on the lowest rotational levels of the $X\,^2\Sigma_g^+\,(v^+ = 0)$ ground state of H_2^+ and extrapolation to the series limit. The $np1_1\,(0, 0)$ series of π^- electronic character converging on the ground state of ortho H_2^+ was found to be the most suitable, because this series is the least perturbed low-ℓ series and the positions of the levels in the range $n =$ 54–64 with respect to the ionisation thresholds are known with an accuracy of better than 100 kHz from millimetre-wave spectroscopic experiments and multichannel quantum defect theory [12,10]. To label the Rydberg series we use the notation $n\ell N_N^+(v^+, S)$. N and N^+ are the total angular momentum quantum numbers excluding spins of H_2 and H_2^+, respectively. N is the quantum number resulting from the vector addition $\vec{N}^+ + \vec{\ell}$, $\vec{\ell}$ being the orbital angular momentum of the Rydberg electron. In the present case, $v^+ = 0$ and $S = 0$ so that we usually omit these quantum numbers in the labels.

In our previous work [11], we determined the position of the $np1_1$ levels with respect to the ground state of ortho H_2 as a sum of the intervals between the ground state and the $EF\,^1\Sigma_g^+\,(v = 0, N = 1)$ state from Ref. [13] and between the $EF\,^1\Sigma_g^+\,(v = 0, N = 1)$ state and the $np1_1$ level (see Figure 1a). A disadvantage of this method is that the frequency required to pump the $X \rightarrow EF$ two-photon transition is high enough to ionise the *EF* state, which leads to the generation of ions in the measurement volume. These ions, in turn, induce inhomogeneous line broadenings and line shifts, which eventually limits the accuracy of the measurement of the ionisation and dissociation energies to about 10 MHz.

This problem can be overcome by determining the interval between the $3d\sigma\,GK\,^1\Sigma_g^+\,(v = 1, N = 1)$ state [designated $GK\,(v = 1, N = 1)$ hereafter] and the $np1_1$ level after excitation to the $GK\,(v = 1, N = 1)$ state in a resonant two-photon excitation via the $B\,^1\Sigma_u^+\,(v = 3, N = 2)$ state (see Figure 1c), and measuring the interval between the $GK\,(v = 1, N = 1)$ state and the ground state by Doppler-free two-photon spectroscopy in a separate experiment (see Figure 1b). The lifetime of the $GK\,(v = 1, N = 1)$ state is long enough (≈25 ns; [14–16]) so that the interval can be determined with a precision of ≈1 MHz by near-infrared (NIR) laser spectroscopy. The disadvantage of this scheme is that the frequency needed to measure the *X*–*GK* interval by two-photon spectroscopy lies in the vacuum–ultraviolet (VUV), but recent progress in VUV frequency combs [17,18] suggests that such a measurement should be possible.

In this article, we report a measurement of the frequency of the transition from the $GK\,(v = 1, N = 1)$ state to the $np1_1$ level following the excitation scheme of Figure 1(c) at an accuracy of 1.2 MHz and describe in detail how the systematic errors arising from ac Stark shifts and dc Stark shifts were quantified and minimised.

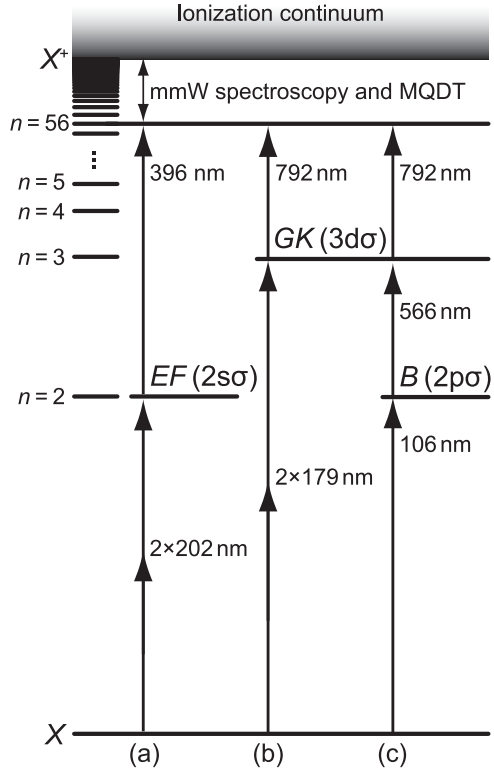


Figure 1. Schematic energy-level diagram of selected electronically excited states of molecular hydrogen (not to scale) with possible excitation schemes to access the 56*p* Rydberg state. The values given next to the arrows are the wavelengths necessary to excite the corresponding transition (see text for details).

2. Experiment

The measurement of the $GK(v = 1, N = 1) \rightarrow 56p1_1$ transition of H_2 relied on the excitation sequence

$$X\,(v = 0, N = 1) \rightarrow B\,(v = 3, N = 2) \rightarrow GK(v = 1, N = 1) \rightarrow 56p1_1. \quad (1)$$

The pulsed VUV radiation used to drive the $X \rightarrow B$ transition was generated by resonance-enhanced sum-frequency mixing in Xe using two Nd:YAG-pumped dye lasers, as described in detail in Ref. [12]. The visible radiation needed for the $B \rightarrow GK$ transition was produced by a dye laser pumped by the same Nd:YAG laser. The experiment was carried out at a repetition rate of 25 Hz. The durations of the VUV and visible-laser pulses were about 2 and 5 ns, respectively.

The narrow-band NIR radiation employed for the precision measurement of the $GK \rightarrow 56p1_1$ transition was generated by a home-built laser system described in Ref. [19] which produces near-Fourier-transform-limited pulses with

a pulse length that can be adjusted in the range between 10 ns and 1 μs. The pulses were chopped out of the continuous-wave output of a Ti:Sa ring laser using an acousto-optic modulator (AOM) operated in a pulsed mode at a driving frequency of 1 GHz. The weak pulses of NIR radiation (pulse energy in the range 1–10 nJ) emitted in the first diffraction order of the AOM were amplified to pulse energies of several mJ in Ti:Sa crystals using two successive amplifiers operated in a travelling multipass configuration (see Ref. [19] for details).

The vacuum chamber in which photoexcitation was carried out is depicted schematically in Figure 2. The H_2 molecules were introduced into the photoexcitation region by means of a pulsed valve operated at a stagnation pressure of 3 bar. The supersonic beam resulting from the adiabatic expansion in vacuum was collimated using two skimmers before entering the excitation region consisting of a cylindrically symmetric stack of six resistively coupled metallic plates (called electrodes hereafter) designed for the application of homogeneous electric fields. In the middle of this region, the molecular beam was intersected at right angles by the VUV, visible and NIR laser beams. The visible-laser beam and the NIR laser beam labelled '1' in Figure 2 were recombined using a dichroic mirror before entering the chamber. The VUV laser beam crossed these two beams at right angles and the small volume defined by the interaction of the three laser beams and the molecular beam was located on the axis of the electrode stack. The polarisation vectors of the visible and VUV laser radiation were parallel, and the polarisation of the NIR radiation was perpendicular, to the molecular-beam propagation axis.

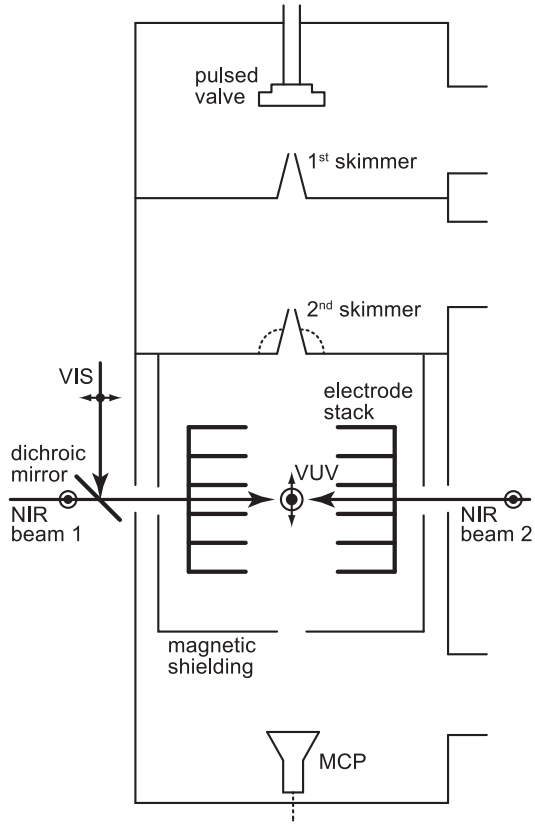


Figure 2. Schematic diagram of the experimental chamber. At the position where the laser beams intersect the molecular beam, the polarisations of the VUV and visible-laser beams are parallel to the propagation axis of the molecular beam, and the polarisation of the NIR laser beams is perpendicular to the plane spanned by the propagation axes of the molecular beam and the NIR laser beams (see text for details).

The photoexcitation region was surrounded by two concentric magnetic shields made of mumetal to suppress stray magnetic fields in the photoexcitation volume. The cylindrical geometry of the excitation region was chosen to ensure that the stray electric field components perpendicular to the axis of the electrode stack are negligible (i.e. less than 1 mV/cm) in the region close to the symmetry axis.

The transitions to the $56p1_1$ Rydberg states of H_2 were detected by delayed pulsed field ionisation followed by the extraction of the H_2^+ ions towards a microchannel-plate detector via a field-free time-of-flight tube. The last plate of the electrode stack on the detector side was earthed and the field-ionisation pulses were produced by applying a positive voltage to the plate located on the pulsed-nozzle side (see Figure 2). The spectra were obtained by monitoring the field-ionisation yield as a function of the NIR frequency. To separate the ions produced by photoionisation of the *GK* state with the visible laser from those produced by delayed pulsed field ionisation, a weak electric field pulse was applied immediately after the (field-free) photoexcitation and was maintained until the application of the larger electric field pulse used for field ionisation. To avoid stray electric fields caused by ions in the photoexcitation volume, the intensity of the visible laser was strongly attenuated (to less than 10 μJ/pulse) when the precision measurements were carried out.

The frequency of the NIR radiation was calibrated by splitting off a fraction of the cw output of the Ti:Sa ring laser to record a Doppler-free spectrum of I_2 for the determination of absolute frequencies and the transmission through an etalon of 149.969(1) MHz free spectral range for the determination of relative frequencies (see Ref. [11] for details). The a_1 component of the $X(v'' = 15, J'' = 62) \rightarrow B(v' = 0, J' = 63)$ transition of I_2 at 12635.698110(3) cm^{-1} [20] was used because it is located in the immediate vicinity of the $GK \rightarrow 56p1_1$ transition of H_2 (see Figure 5 below). The pressure shift of $-0.4(0.3)$ MHz of the iodine transitions in our cell was included in the calibration procedure. The value of this shift was determined as explained in Ref. [11] by comparing the frequencies of seven transitions measured with an iodine cell identical to the one used in the present work and frequencies reported in Ref. [20]. To measure the Doppler shift of the transitions, the pulse-amplified NIR laser beam was split into two beams

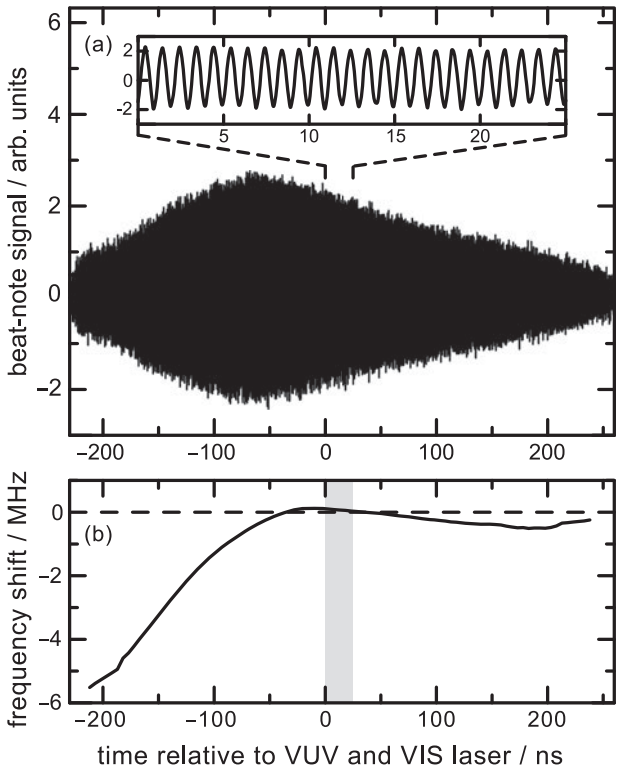


Figure 3. (a) Beat-note signal arising from the superposition of the cw output of the NIR ring laser with an amplified NIR laser pulse. The oscillation frequency of 1 GHz corresponds to the frequency of the accousto-optic modulator used to generate a seed pulse from the cw output of the ring laser. (b) Evolution of the frequency shift caused by the pulse amplification determined from the beat-note signal. The $GK\,(v=1, N=1)$ state is excited at time 0 and the grey area represents its lifetime of ≈25 ns [14,15]. The horizontal dashed line indicates the nominal frequency (i.e. without any chirp) of the NIR laser.

with a beam splitter and the two beams (labelled 1 and 2 in Figure 2) were introduced into the chamber from opposite sides. The transition was measured for both beams in the same scan and the Doppler shift was determined as half the separation between the two Doppler components.

The pulse amplification of the chopped NIR beam is accompanied by a frequency chirp resulting from time-dependent changes of the refractive index of the Ti:Sa crystals. To quantify the frequency evolution during a pulse, we followed the procedure described in [19]. The pulse-amplified NIR beam and the cw output of the NIR ring laser were recombined and overlapped on the active area of a fast photodiode. The resulting beat pattern for a 200 ns (full width at half-maximum) NIR pulse is depicted in Figure 3(a). The interference signal oscillates with a beat frequency of ≈1 GHz which corresponds to the AOM driving frequency (1 GHz) (see inset). The difference between the observed beat frequency and the AOM driving frequency can be expressed as a time-dependent phase function. The time-dependent frequency chirp was numerically calculated as the time derivative of the phase function following the method described in Ref. [21]. The reconstructed frequency evolution, which was reproducible for all pulses of this length, is displayed in Figure 3(b). The frequency shift evolves from an initial value of −6 MHz immediately after the Nd:YAG pulse to about zero in the first 200 ns and then oscillates around zero. To reduce the effects of the frequency chirp on the high-resolution measurements, the laser pulses used for the excitation to the $GK\,(v=1, N=1)$ state were fired at time 0 in Figure 3(b), when the NIR-frequency shift is negligible. The increasing shift at later times (≈50 ns) had no incidence on the measurement because it takes place on a timescale longer than the lifetime of ≈25 ns [14–16] of the $GK\ (v=1, N=1)$ state, which is indicated by the area shaded in grey in Figure 3(b). These chirp-free conditions were confirmed for each measurement presented in Section 3 by carrying out the analysis described above. We nevertheless included a systematic uncertainty of 0.5 MHz in the NIR frequency arising from the frequency chirp.

3. Results

One of the major difficulties in the measurement of the frequency of the $GK\,(v=1, N=1) \rightarrow 56p1_1\,(v^+=0, S=0)$ transition lies in the quantification of systematic errors originating from ac and dc Stark shifts caused by the laser fields and by electric stray fields, including those caused by ions generated in the measurement volume. Indeed, the polarisability of Rydberg states scales as the seventh power of the principal quantum number n and even small stray electric fields can shift the frequencies of transitions to high Rydberg states. Moreover, the n^{-3} scaling of the photoexcitation cross section requires strong laser intensities which inevitably lead to ac Stark shifts.

Because of the cylindrical symmetry of the electrode stack surrounding the excitation volume, the stray electric field components perpendicular to the symmetry axis are negligible (see below and also Section 2). The stray field thus points along the axis of propagation of the supersonic beam and of the time-of-flight tube (see Figure 2). To determine the stray field, we follow the procedure described in detail in Ref. [22], which consists of measuring the shifts of the transition frequency upon application of well-defined electric fields across the electrode stack. At low values of the electric field, the Stark shifts are smaller than the spectral width of about 20 MHz (see Figure 4a). With increasing field strength, the line shifts and splits into two components corresponding to Rydberg states with M_N values of 0 and ± 1. The corresponding Stark shifts are plotted as a function of the applied electric field in Figure 4(c). By minimising the least-squares deviation between the observed Stark shifts (black dots) and Stark shifts calculated with the method described in Ref. [23] (full lines), the compensation field was determined to be 24.6(6) mV/cm, and the

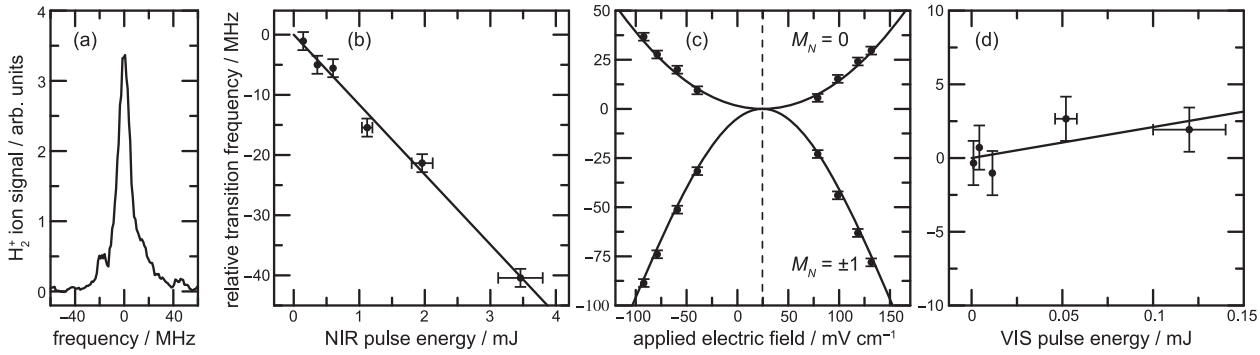


Figure 4. (a) Spectrum of the $GK(v = 1, N = 1) \rightarrow 56p1_1\,(v^+ = 0, S = 0)$ transition in H_2 near 12635.7 cm^{-1} and shifts of the transition frequency as a function of (b) the pulse energy of the NIR laser, (c) the dc electric field applied in the direction parallel to the polarisation vector of the VUV laser radiation, and (d) the pulse energy of the visible laser. The straight lines in panels (b) and (d) were obtained by linear regression and have slopes of −11.6(7) MHz/mJ and 21(20) MHz/mJ, respectively. The dashed line in panel (c) indicates the field [24.6(6) mV/cm] which compensates the stray field.

uncertainty in the transition frequency resulting from the 0.6 mV/cm uncertainty of the compensation field was found to be 0.1 MHz. Analysing the data presented in Figure 4(c), including the possibility of a stray field component perpendicular to the molecular beam axis, leads to the conclusion that this component must be less than 0.3 mV/cm and thus negligible.

To quantify the ac Stark shifts induced by the NIR laser field, the transition frequency was measured for several NIR pulse energies up to 3.4 mJ/pulse, as depicted in Figure 4(b). A linear regression of these data led to a slope of −11.6(7) MHz/mJ. The final measurements of the transition frequencies were carried out at an average NIR pulse energy of 40 μJ, resulting in a systematic shift of −0.4(6) MHz, the large uncertainty arising from the strong pulse-to-pulse energy fluctuations of the NIR laser.

Initially, we expected that the visible laser used to prepare the initial population in the $GK(v = 1, N = 1)$ level would not cause any shift of the transition frequency because the duration of the visible-laser pulses (5 ns) was much shorter than the lifetime (≈25 ns) of the $GK(v = 1, N = 1)$ state and the NIR pulse duration (300 ns). Nevertheless, a dependence (21(20) MHz/mJ) of the $GK(v = 1, N = 1) \rightarrow 56p1_1$ transition frequency on the visible-laser-pulse energy was observed (see Figure 4(d)), which we attribute to the stray fields caused by ions generated by photoionisation of the $GK(v = 1, N = 1)$ level during the visible-laser pulse. For the final measurements, an average visible-laser-pulse energy of approximately 8 μJ was used, which did not result in any systematic shift, but in an uncertainty of 0.5 MHz.

To minimise the Doppler width of the transition, the propagation axes of the molecular and the NIR laser beams were chosen to be perpendicular. A small Doppler shift of the transition frequency may nevertheless result from a remaining deviation from 90°, or from the selection of molecules with a non-zero velocity component in the direction of propagation of the NIR laser by the VUV and visible lasers used to populate the $GK(v = 1, N = 1)$ state. To determine this Doppler shift, the final measurements were performed after dividing the NIR beam into two components using a 50% beam splitter and directing these two beams into the measurement region in a counterpropagating arrangement (see Figure 2). A typical spectrum measured in this configuration is displayed in Figure 5(a), and consists of two lines, labelled 1 and 2 to designate the NIR beam responsible for the absorption (see inset of Figure 5). The Doppler shift corresponds to half the separation of the two lines, and the transition frequency can be determined by taking the average of the positions of the two lines.

The NIR laser frequency was determined as described in Section 2 using the a_1 component of the $X(v'' = 15, J'' = 62) \rightarrow B(v' = 0, J' = 63)$ transition of I_2 at 12635.698110(3) cm^{-1} (378808699.5(1) MHz) [20] for the absolute frequency calibration and the transmission spectrum through an etalon having a free spectral range of 149.969(1) MHz for the determination of relative frequencies. As illustration, the Doppler-free I_2 and etalon transmission spectra recorded simultaneously with the spectrum of the $GK(v = 1, N = 1) \rightarrow 56p1_1\,(v^+ = 0, S = 0)$ transition are displayed in Figure 5(c) and 5(b), respectively. The I_2 lines measured with our I_2 cell are subject to a pressure shift of −0.4(3) MHz, so that the I_2 line observed in Figure 5(c) has a central frequency of 378808699.1(3) MHz.

To determine the central frequency, each Doppler component was modelled by taking into account the hyperfine structure of the $56p1_1\,(v^+ = 0, S = 0)$ level as measured in Ref. [12]. The intensities of the (unresolved) transitions to the $F = 0$, 1 and 2 hyperfine-structure components were given weights of 1, 3 and 5, respectively, resulting in the stick spectra depicted in Figure 5(a). The stick spectra were then convoluted using a Gaussian line-shape function.

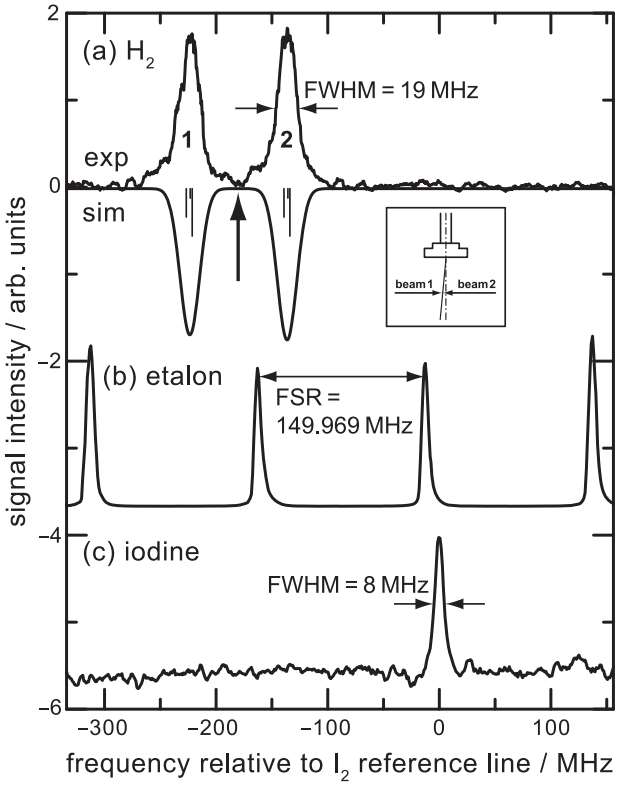


Figure 5. (a) Experimental and simulated (inverted trace) spectrum of the $GK(v = 1, N = 1) \rightarrow 56p1_1(v^+ = 0, S = 0)$ transition in H_2. The two lines in the H_2 spectrum correspond to the two Doppler components originating from the two counterpropagating NIR laser beams labelled 1 and 2 in the inset. The actual transition frequency is indicated by the vertical arrow. The stick spectrum shows the hyperfine structure of the $56p1_1(v^+ = 0, S = 0)$ level as measured in Ref. [12] and was convoluted by a Gaussian line-shape function with a full width at half-maximum of 18 MHz to obtain the simulated spectrum. (b) Transmission spectrum through an etalon for the determination of relative frequencies. (c) Doppler-free spectrum of molecular iodine showing the a_1 component of the $X(v'' = 15, J'' = 62) \rightarrow B(v' = 0, J' = 63)$ transition at 12635.698110(3) cm^{-1} [20] used to determine absolute frequencies. Traces (b) and (c) were shifted along the vertical axis for clarity.

The full width at half-maximum of the lines and the central positions were determined in a least-squares fit. We estimate the uncertainty resulting from our line-shape model to be 0.1 MHz.

The pressure shift of the transition was estimated to be negligible at the H_2 density in the photoexcitation volume (about 10^{13} cm^{-3}) using the pressure-shift coefficient of Rydberg states of H_2 reported by Herzberg and Jungen [24] [5.7 ± 0.5 cm^{-1}/amagat] (see also discussion in Ref. [11]).

The results of 10 measurements carried out on different days after realignment of the lasers are summarised in Figure 6, which shows the positions of the two Doppler components as the filled squares and triangles, and their average as the filled circles. The dashed line indicates the

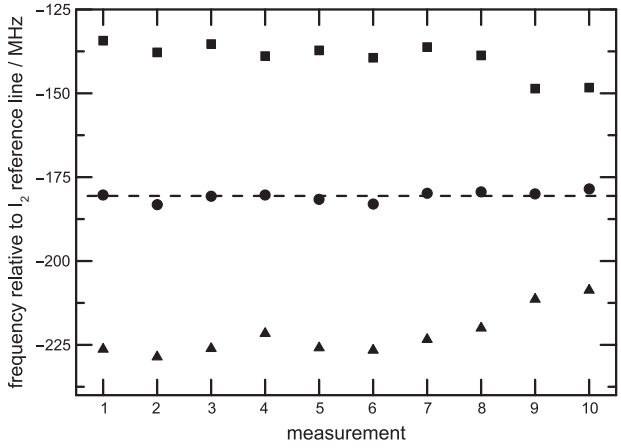


Figure 6. Distribution of the measured frequency of the $GK(v = 1, N = 1) \rightarrow 56p1_1(v^+ = 0, S = 0)$ transition. The triangles and squares represent the positions of the lines corresponding to the two Doppler components observed in the spectra and the circles mark their mean values. The final result is indicated by the dashed line. The standard deviation of the measurement is represented by the size of the circles.

position relative to the I_2 calibration line of the average of the 10 central frequencies [−180.8(6) MHz]. The standard deviation of 0.6 MHz of these measurements was assumed to be representative of the statistical error of our measurement and is limited by the Doppler width of the lines.

Table 1 lists all contributions to our determination of the $GK(v = 1, N = 1) \rightarrow 56p1_1(v^+ = 0, S = 0)$ transition frequency and their estimated uncertainties. The final result is 378809478.7(12) MHz [12635.72410(4) cm^{-1}].

4. Discussion and conclusions

The measurements presented in this article demonstrate that the frequencies of transitions between low and high Rydberg states can be determined by NIR laser spectroscopy with a relative accuracy $\Delta\nu/\nu$ of 3×10^{-9} and an absolute accuracy of 1.2 MHz. This accuracy is primarily limited by the uncertainty in the ac Stark shift and by the statistical uncertainty associated with the determination of the centres of the Doppler-broadened lines (full width at half-maximum of about 20 MHz).

From the measurement of the $GK(v = 1, N = 1) \rightarrow 56p1_1$ transition frequency presented in this article, further intervals can be derived, as summarised in Table 2. The position of the $56p1_1(v^+ = 0, S = 0)$ Rydberg state of ortho H_2 with respect to the centre of gravity of the hyperfine structure of the $X^+(v^+ = 0, N^+ = 1)$ ground state of ortho H_2^+ has been determined to be −1045709.62(10) MHz by analysing millimetre-wave spectra with multichannel quantum defect theory [10]. By subtracting this (negative) frequency from the frequency of the $GK(v = 1, N = 1) \rightarrow 56p1_1$ transition, one obtains the value of 379855188.3(12) MHz for the ionisation energy of the $GK(v = 1, N = 1)$ state of ortho H_2. The position of the $GK(v = 1, N = 1)$

Table 1. Determination of the $GK(v = 1, N = 1) \rightarrow 56p1_1(v^+ = 0, S = 0)$ transition frequency and error budget (all values in MHz). The transition frequency corresponds to the centre of gravity of the hyperfine structure. The total uncertainty was determined by summation of the individual uncertainties in quadrature.

	Shift	Uncertainty
Transition frequency relative to the I_2 reference line	−180.8	0.6
Position of the I_2 reference line [20]	378808699.5	<0.1
Pressure shift of the I_2 reference line	−0.4	0.3
Uncertainty of the free spectral range	0.0	<0.1
Frequency shift in the Ti:Sa amplifier	0.0	0.5
ac Stark shift by the NIR laser	0.4	0.6
dc Stark shift by the residual stray electric field	0.0	0.1
Frequency shift by the VIS laser	0.0	0.5
Pressure shift	0.0	<0.1
Uncertainty of the line-shape model	0.0	0.1
Shift by AOM used in the iodine spectroscopy	−40.0	<0.1
Shift by AOM used to generate the seed pulse	1000.0	<0.1
Total	378809478.7	1.2

Table 2. Determination of the ionisation energy and the term value of the $GK(v = 1, N = 1)$ state of H_2. The frequencies and wavenumbers correspond to the centre of gravity of the hyperfine structure.

Label	Energy interval	Frequency/MHz	Wave number/cm^{-1}	Reference
(1)	$GK(v = 1, N = 1)$–$56p1_1(v^+ = 0, S = 0)$	378809478.7(12)	12635.72410(4)	This work
(2)	$56p1_1(v^+ = 0, S = 0)$ –$X^+(v^+ = 0, N^+ = 1)$	1045709.62(10)	34.881118(3)	[10]
(3)[1]	$GK(v = 1, N = 1)$ –$X^+(v^+ = 0, N^+ = 1)$	379855188.3(12)	12670.60522(4)	This work
(4)	$X^+(v^+ = 0, N^+ = 0)$ –$X^+(v^+ = 0, N^+ = 1)$	1745801.660(3)	58.2336751(1)	[25–27]
(5)[2]	$GK(v = 1, N = 1)$ –$X^+(v^+ = 0, N^+ = 0)$	378109386.6(12)	12612.37154(4)	This work
(6)	$X(v = 0, N = 0)$ –$X(v = 0, N = 1)$	3552146(3)	118.48684(10)	[28]
(7)	$X(v = 0, N = 1)$ –$X^+(v^+ = 0, N^+ = 1)$	3728136204(11)	124357.23797(36)	[11]
(8)[3]	$X(v = 0, N = 0)$ –$GK(v = 1, N = 1)$	3351833162(12)	111805.1196(4)	This work
			111805.1101(10)	[29]
			111805.139(17)	[30]

[1]Ionisation energy of the $GK(v = 1, N = 1)$ state, determined as (1) + (2). [2]Determined as (3) − (4). [3]Term value of the $GK(v = 1, N = 1)$ state, determined as (6) + (7) − (3).

state with respect to the $X^+(v^+ = 0, N^+ = 0)$ ground state of H_2^+ can further be determined to be −378109386.6(12) MHz by including the frequency of 1745801.660(3) MHz [25–27] corresponding to the energy difference between the centre of gravity of the $X^+(v^+ = 0, N^+ = 1)$ state and the $X^+(v^+ = 0, N^+ = 0)$ state.

The present measurement of the ionisation energy of the $GK(v = 1, N = 1)$ state could be used to derive an improved value of the dissociation and ionisation energies of H_2 if a precision measurement of the $X(v = 0, N = 1)$–$GK(v = 1, N = 1)$ interval is carried out. The current uncertainty in the ionisation energy of H_2 is 11 MHz [11] and the experimental result is in agreement with *ab initio* calculations which include QED corrections up to the leading one-loop member of the α^4 term [5] within the combined uncertainties of 30 MHz of the experimental and theoretical determinations. The present results suggest that it should be possible to reduce the experimental uncertainty of the ionisation and dissociation energies of H_2 by a factor of almost 10 in the near future.

In the meantime, the ionisation energy of the $GK(v = 1, N = 1)$ state listed above can be combined with the value of 3728136204(11) MHz determined recently for the ionisation energy of ortho H_2 [i.e. the $X(v = 0, N = 1)$–$X^+(v^+ = 0, N^+ = 1)$ interval] [11] and the value of 3552146(3) MHz known for the $X(v = 0, N = 0)$–$X(v = 0, N = 1)$ interval [28] to obtain the term value of 3351833162(12) MHz [111805.1196(4) cm^{-1}] of the $GK(v = 1, N = 1)$ state. This value deviates from the value of 111805.1101(10) cm^{-1} reported in Ref. [29] but is in good agreement with, and more precise than, the older result of 111805.139(17) cm^{-1} obtained by Jungen *et al.* [30].

Acknowledgements

This article is dedicated to Professor Martin Quack whom we thank for his interest in our work, for his stimulating influence and for fruitful scientific exchanges over many years. We thank Professor Horst Knöckel (University of Hannover) for his advice concerning pressure shifts of the I_2 calibration lines and Professor

Wim Ubachs (Free University of Amsterdam) for a useful discussion concerning possible origins of the discrepancy between the term value of the $GK(v = 1, N = 1)$ state reported in this article and that reported in Ref. [29]. We also thank Josef A. Agner, Guido Grassi, Urs Hollenstein, and Hansjürg Schmutz for their help in the construction of the new setup for the iodine spectroscopy. This work is supported financially by the Swiss National Science Foundation under project 200020-135342 and by the European Research Council advanced grant program under project 228286.

References

[1] M. Quack, Faraday Discuss. **150**, 533 (2011).
[2] W.E. Lamb, and R.C. Retherford, Phys. Rev. **72**, 241 (1947).
[3] D.M. Kara, I.J. Smallman, J.J. Hudson, B.E. Sauer, M.R. Tarbutt, and E.A. Hinds, New J. Phys. **14**, 103051 (2012).
[4] M. Quack, *Fundamental Symmetries and Symmetry Violations from High-Resolution Spectroscopy* in *Handbook of High-Resolution Spectroscopy*, edited by Martin Quack and Frédéric Merkt (John Wiley & Sons, Chichester, 2011), Vol. **1**.
[5] K. Piszczatowski, G. Łach, M. Przybytek, J. Komasa, K. Pachucki, and B. Jeziorski, J. Chem. Theory Comput. **5**, 3039 (2009).
[6] W. Kolos, and C.C.J. Roothaan, Rev. Mod. Phys. **32**, 219 (1960).
[7] L. Wolniewicz, J. Chem. Phys. **45**, 515 (1966).
[8] L. Wolniewicz, J. Mol. Spectrosc. **169**, 329 (1995).
[9] K. Pachucki, and J. Komasa, Phys. Chem. Chem. Phys. **12**, 9188 (2010).
[10] D. Sprecher, Ch. Jungen, W. Ubachs, and F. Merkt, Faraday Discuss. **150**, 51 (2011).
[11] J. Liu, E.J. Salumbides, U. Hollenstein, J.C.J. Koelemeij, K.S.E. Eikema, W. Ubachs, and F. Merkt, J. Chem. Phys. **130**, 174306 (2009).
[12] A. Osterwalder, A. Wüest, F. Merkt, and Ch. Jungen, J. Chem. Phys. **121**, 11810 (2004).
[13] S. Hannemann, E.J. Salumbides, S. Witte, R.T. Zinkstok, E.J. van Duijn, K.S.E. Eikema, and W. Ubachs, Phys. Rev. A **74**, 062514 (2006).
[14] R.L. Day, R.J. Anderson, and F.A. Sharpton, J. Chem. Phys. **71**, 3683 (1979).
[15] J.A. Sánchez, and J. Campos, J. Phys. France **49**, 445 (1988).
[16] P. Quadrelli, K. Dressler, and L. Wolniewicz, J. Chem. Phys. **93**, 4958 (1990).
[17] R.Th. Zinkstok, S. Witte, W. Ubachs, W. Hogervorst, and K.S.E. Eikema, Phys. Rev. A **73**, 061801(R) (2006).
[18] D.Z. Kandula, Ch. Gohle, T.J. Pinkert, W. Ubachs, and K.S.E. Eikema, Phys. Rev. Lett. **105**, 063001 (2010).
[19] R. Seiler, Th. Paul, M. Andrist, and F. Merkt, Rev. Sci. Instr. **76**, 103103 (2005).
[20] E.J. Salumbides, K.S.E. Eikema, W. Ubachs, U. Hollenstein, H. Knöckel and E. Tiemann, Eur. Phys. J. D **47**, 171 (2008); H. Knöckel, B. Bodermann and E. Tiemann, Software IodineSpec 5 (2008).
[21] M. Takeda, H. Ina, and S. Kobayashi, J. Opt. Soc. Am. **72**, 156 (1982).
[22] A. Osterwalder, and F. Merkt, Phys. Rev. Lett. **82**, 1831 (1999).
[23] Ch. Seiler, S.D. Hogan, and F. Merkt, Phys. Chem. Chem. Phys. **13**, 19000 (2011).
[24] G. Herzberg and Ch. Jungen, J. Mol. Spectrosc. **41**, 425 (1972).
[25] V.I. Korobov, Phys. Rev. A **74**, 052506 (2006).
[26] V.I. Korobov, Phys. Rev. A **73**, 024502 (2006).
[27] V.I. Korobov, Phys. Rev. A **77**, 022509 (2008).
[28] D.E. Jennings, A. Weber, and J.W. Brault, J. Mol. Spectrosc. **126**, 19 (1987).
[29] D. Bailly, E.J. Salumbides, M. Vervloet, and W. Ubachs, Mol. Phys. **108**, 827 (2010).
[30] Ch. Jungen, I. Dabrowski, G. Herzberg, and M. Vervloet, J. Chem. Phys. **93**, 2289 (1990).